# Equations to Fit Partially Supported Jets in Models of Dam Breach

Donald L. Baker [1]


## Abstract

Head-discharge equations are fitted to a set of physical models of dam breach for the cases where there is a drop below the jet but apparently no aeration. Investigations with simulated annealing and a commercial curve-fitting program suggest that the reductions in flow from that of a free-falling, aerated jet can be fitted with equations in a dimensionless scaling system derived from the Buckingham Pi theorem and integration of the ideal weir equation. A set of linear corrections are fitted to data for a breach width of 0.406m and applied to data for breach widths of 0.203m and 0.813m, to check scaling.



## Author

[1] Ph.D. Soil Physics, 5001 West 5th Place, Stillwater, OK 74074-6703



## Keywords

Dam breach, head-discharge, physical model, simulated annealing, Buckingham Pi, partially supported jet

## Scope of the paper

It is always more satisfying to develop explicit analytic equations from first principles, but the author is not yet qualified to do that in this field. Therefore the scope of this work is limited to the application of simple weir flow concepts that are fitted to the data set by curve fitting and simulated annealing. Only the discharge coefficients are fitted. All other secondary effects, such as contraction, entrance velocity corrections and boundary layers are ignored, partly due as well to the limitations of the data set, for which only six head-discharge points were typically taken per geometry. While one may not be an expert in a field, it is nevertheless possible to consider basic equations and apply methods such as simulated annealing (Goffe, et al., 1994) that work across many disciplines. If the concept of a partially-supported jet is addressed elsewhere in the literature, perhaps under another term, the author was not able of find it in the computerized title and abstract databases available through a local university library. One can only apologize if relevant work has not been considered or cited.

## The physical model

Consider the case of water flowing in a trapezoidal notch through the trapezoidal embankment of a reservoir in Figure 1. The notch has a bottom width, b (units of length, L), at height, hu (L), above the reservoir floor, with a sidewall angle of $\phi$ (rad) from the vertical, making a slope, ms, horizontal to vertical (H:V). The embankment has an upstream angle of $\theta$ (rad) above the horizontal, making a slope, mu (H:V). The intersection of the notch with the upstream slope, especially the horizontal part, is called the crest of the resulting weir. In addition, the floor of the notch downstream of the crest can be dropped, hh (L), below the crest, forming a rectangular channel below the crest, so that the water flowing into it can be an aerated waterfall, or nappe. Figure 1 shows one such condition with hh = hu. Vertical

measurements are taken with respect to the elevation of the bottom width, b, with hh and hu positive downwards.

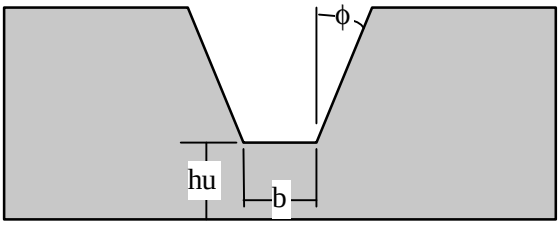


Figure 1a: View from Upstream

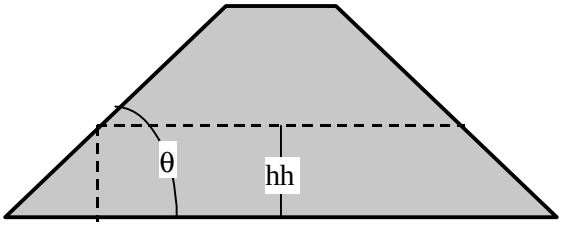


Figure 1b: Side View

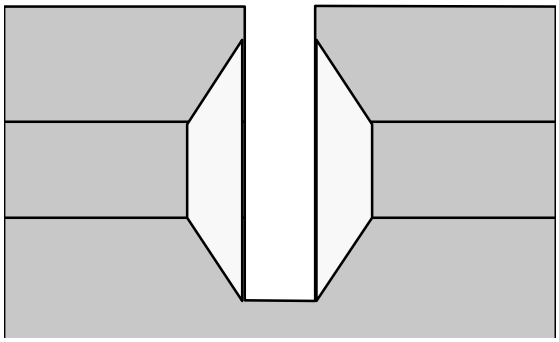

Figure 1c: Top View

This model was built and run at the Hydraulic Engineering Research Unit of the USDA Agricultural Research Service, Stillwater, OK. It was demonstrated in one geometry on June 27, 2001, to participants of the FEMA sponsored Workshop on Issues, Resolutions, and Research Needs Related to Dam Failure Analyses, Oklahoma City, OK. Three sets of data were generated. In the largest set the geometry combinations are: b = 0.406m (16 in); hu = 0 m, 0.152 m (0.5 ft), 0.305 m (1 ft); mu = 0, 1, 2, 2.5, 3, 4, 6; hh = 0 m, 0.152 m (0.5 ft), 0.305 m (1 ft); and ms = 0, 0.25, 0.5, 1, 1.5, 2. Two other sets were created to check scaling. For b = 0.203 m (8 in), the variations are: hu = 0 m, 0.152 m (0.5 ft), 0.305 m (1 ft); mu = 3; hh = 0 m, 0.152 m (0.5 ft), 0.305 m (1 ft); and ms = 0, 0.25, 0.5, 1, 1.5, 2. For b = 0.813 m

(32 in), the variations are: hu = 0 m, 0.305 m (1 ft); mu = 3; hh = 0 m, 0.152 m (0.5 ft), 0.305 m (1 ft); and ms = 0.5.

Only two hydraulic measurements were made, the elevation, he (m), positive upwards above the crest of the notch of the upstream reservoir, and the bulk flow of water, Q ($m^3/s$), through the notch. Flow was measured with a differential manometer connected to orifice plates in a 0.3048 m (12 in) inlet pipe. The flow was typically set to six approximate levels of Q = 0.00354, 0.00708, 0.01416, 0.02832, 0.05664, 0.08496, 0.1133, 0.1699, 0.2266 or 0.3682 ($m^3/s$) (0.125, 0.25, 0.5, 1, 2, 3, 4, 6, 8 or 13 cfs), depending on the size of the notch. Then reservoir elevation was measured with point gage in a stilling well connected to a diffusing pipe on the bottom of the flume upstream of the Bernoulli drop at the notch.

## Review of previous work

Previously (Baker, 2002), dimensionless equations were fitted to parts of this data for the cases where flow in the notch channel is fully supported by the floor, hh = 0, and where the flow is through a free-falling, aerated jet. In this paper, the terms “fully supported” and “aerated”, respectively, refer to those cases. The fully supported case includes applications already examined by Fread (1984, 1991). To review, the integration of the ideal weir equation (1) (John and Haberman, 1988; Gupta, 1989) was integrated over the geometric break lines of the model, the horizontal breach width and the inclined intersections of the upstream embankment slope and the side slopes of the trapezoidal notch.

$$dQ = Cd \cdot \frac{2\sqrt{2g}}{3} \cdot he^{3/2} \cdot ds, \qquad (1)$$

where Q ($m^3/s$) is volumetric flow, Cd (dimensionless) is the empirically-determined discharge coefficient, g is the acceleration of gravity ($m/s^2$), he (m) is the entrance head level above the crest upstream of any Bernoulli drop, and ds (m) is the incremental width of the weir.

If one folds the geometric corrections into the discharge coefficients, c0 and c1, one gets the general result (2). It assumptions that flow lines are parallel to the surface, the head is hydrostatic, the factors of friction, inertia and contraction are neglected, and the velocity of approach is neglected. Some measure of shear, inertia and contraction are brought back in with the empirically-determined discharge coefficients, which are assumed to be constant with flow and head in a given geometry.

$$Q = c0 \cdot \frac{2\sqrt{2g}}{3} \cdot b \cdot he^{3/2} + c1 \cdot \frac{8\sqrt{2g}}{15} \cdot he^{5/2} \qquad (2)$$

If one applies the Buckingham Pi theorem (Logan, 1987) to (2), one can get the linear dimensionless equation (3).

$$p_q = c0 \cdot \frac{2\sqrt{2}}{3} + c1 \cdot \frac{8\sqrt{2}}{15} \cdot p_e = p0 + p1 \cdot p_e,\ p_q = \frac{Q}{\sqrt{g \cdot b^2 \cdot he^3}},\ p_e = \frac{he}{b} \qquad (3)$$

Note that mu and ms are already dimensionless π-variables, based on the ratios of lengths and heights of the upstream and channel side slopes. In addition, two more p-variables are defined: πu (or piu) = hu/b and πh (or pih) = hh/b for use in the fitting process. Using (3) the experimental data for b = 0.406m was divided into two groups, that for which the jet is fully supported, hh = 0, and that for which the jet is obviously fully aerated, hh > 0, as determined

by the lack of deviation from (3). For these two data sets, c0 and c1 were fitted as functions of the dimensionless geometric variables, mu, ms, πu and πh, for aerated flow, πqa (4), and fully supported flow, πqb (5). In this case, the parameters of (4) have been refitted to remove an internal dependency in the previous paper.

$$p_{qa} = \frac{2\sqrt{2}}{3}\cdot\left[d1 + d2\cdot mu + d3\cdot mu^2 + d4\cdot ms + d5\cdot ms^2 + u1(d6)\right] + \frac{8\sqrt{2}}{15}\cdot\left[1 + u2(d11)\right]\cdot\left[d7\cdot mu + d8\cdot mu^2 + d9\cdot ms + d10\cdot ms^2\right]\cdot p_e \quad (4)$$

$$u1 = \begin{cases} d6, & pu = 0 \\ 0, & pu > 0 \end{cases},\ u2 = \begin{cases} d11, & pu = 0 \\ 0, & pu > 0 \end{cases}$$

where d1 = 0.63112, d2 = 0.031013, d3 =-0.0040739, d4 = 0.030513, d5 = -0.021928, d6 = -0.056881, d7 = 0.37263, d8 = 0.033908, d9 = 0.34755, d10 = 0.097554, d11 = 0.033479

$$p_{qb} = \frac{2\sqrt{2}}{3}\cdot\left[d1 + d2\cdot mu + d3\cdot ms + d4\cdot ms^2 + d5\cdot ms^3\right] + \frac{8\sqrt{2}}{15}\cdot\left[d6\cdot mu + d8\cdot ms + d9\cdot ms^2\right]\cdot p_e \quad (5)$$

where d1 = 0.47099, d2 = 0.0029153, d3 = 0.10965, d4 = -0.11202, d5 = 0.029651, d6 = 0.001102, d7 = 0.37215, d8 = 0.036534

The linearity of (3), (4) and (5) with πe makes it easy to see when the data does not conform with the assumptions used in generating the equation. Then, either the data or the assumptions are bad, indicating that the flow has perhaps entered an regime not explained by the equation. In Figure 2, for example, it is clear that the flow conforms to the linearity of (3) for hh = 0 m and for the lower values of πe for hh = 0.15 and 0.31 m. But for the higher

values of he and hh = 0.15 and 0.31 m, the value of πq not only deviates from (3), it reaches a maximum and decreases, exhibiting non-monotonic behavior.

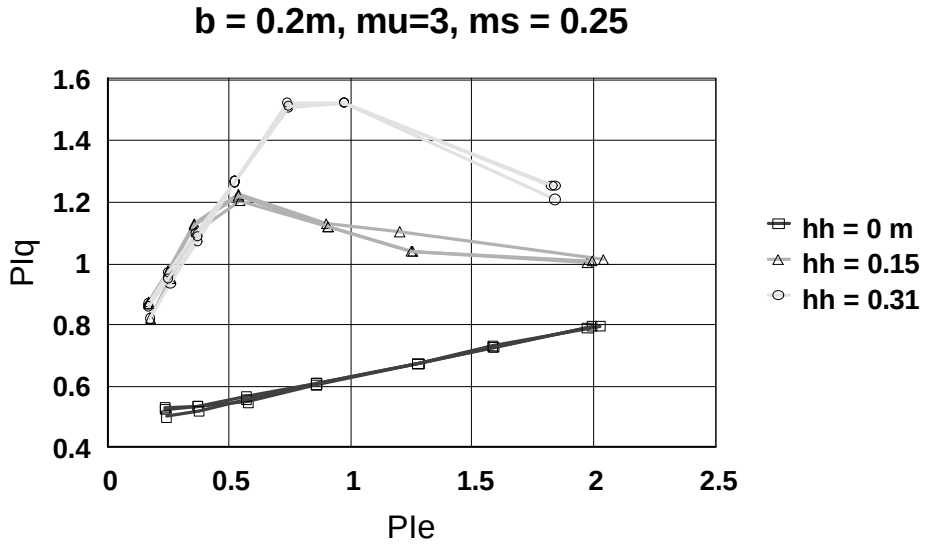


Figure 2: πq versus πe for b = 0.2m, hu = 0, 0.15 and 0.31 m, mu = 3, hh = 0, 0.15 and 0.31 m, and ms = 0.25. Shows the decrease in flow when the jet is supported (hh = 0 m), and when the jet presumably loses aeration.

One might expect this drop; when the entrance head, he, becomes much larger than the modeled head cut drop, hh, the flow should approach fully supported flow in the limit as he goes to infinity. This effect was excluded from the data and neglected in the last paper, and will be addressed here.

**Development**

For a straight drop with simple geometry, Rand (1955) found that the jet lost aeration when the critical depth equaled the height of the drop. Suppose that such a condition does cause the reduction in flow seen at higher heads, he or πe, in some geometries. This is consistent with evidence in the data that shows the effect occurring at higher values of πe for higher values of πh. It would take more flow to cause the rebounding reverse roller behind the

jet to fill in the air pocket for higher drops. So the flow for the aerated condition should be entirely unaffected until the change occurs, then a new flow regime takes over, as in (6)

$$p_q(p_e) = \begin{cases} p_{qa}(p_e) & ,p_e \le p_o \\ p_{qa}(p_e) - p_d(p_e) & ,p_e > p_o \end{cases} \text{, where } \pi o \text{ is a breakpoint} \qquad (6)$$

After a certain amount of trial and error, it becomes apparent that the plot in Figure 3 offers the most promise. It suggests that πd = πqa – πq is strongly linear in πe and modified by the geometry, especially mu.

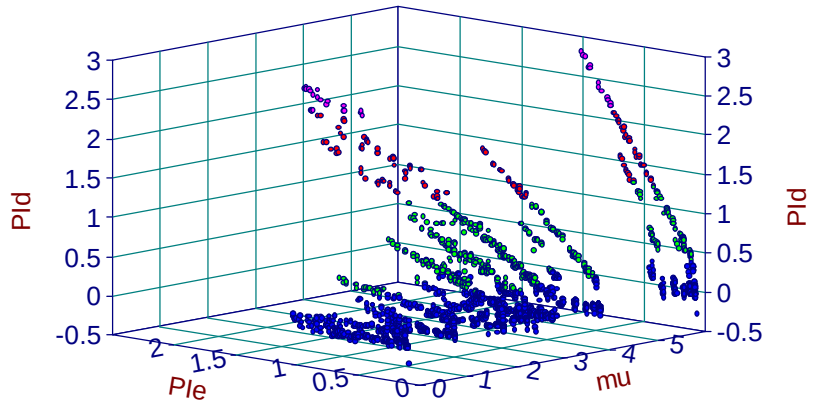


Figure 3: Plot of πd(mu,πe) = πqa-πq for all of the data points in the set of physical models of dam breach

So as a first approximation, we might assume that (6) can be expressed as (7) and see where it leads.

$$p_q = \begin{cases} p_{qa} & ,p_e \le p_o \\ p_{qa} - a(p_e - p_o) & ,p_e > p_o \end{cases} \qquad (7)$$

But the apparent linearity in Figure 3 is partly illusion. It seems the breach side slope, ms, contributes to the variation in πo and α only as a secondary effect. But it is a primary cause of restriction of flow through the breach notch, as shown in equations (4) and (5). This causes considerable variation in the entrance elevation, he, for a given flow, Q. So when the points

due to variation in ms are lumped together in Figure 3, they tend to string out in nearly straight lines. But there is no guarantee that πd is linear with (πe – πo).

We can see this and another problem by plotting πq and πd against πe for equivalent π-scales for b = 0.2 m and 0.4 m. Figure 4a shows measured πq for b = 0.2 m (circles) and 0.4 m (squares), as well as πqb (triangles) from equation (5), versus πe, for mu = 3, ms = 0.25, πu = 0.75 and πh = 0.75. Figure 4b shows πd for b = 0.2 and 0.4 m versus πe for the same geometry.

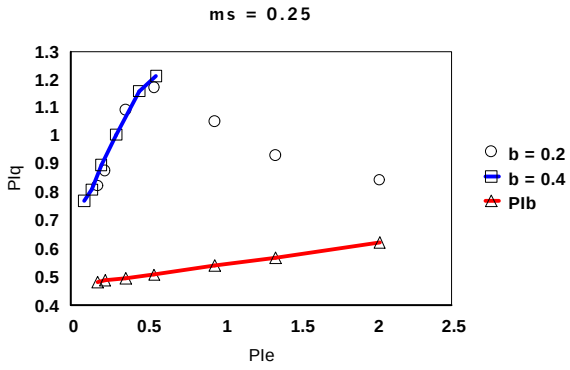


Figure 4a: Comparison of πq(πe) for b = 0.2 and 0.4 m, with mu = 3, ms = 0.25, πu = 0.75 and πh = 0.75

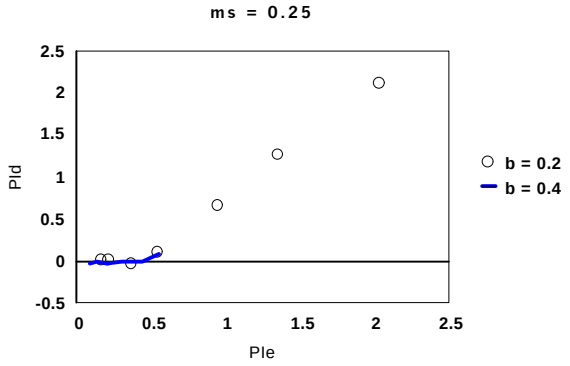


Figure 4b: Comparison of πd(πe) = πqa-πq for b = 0.2 and 0.4 m, with mu = 3, ms = 0.25, πu = 0.75 and πh = 0.75

It seems from Figure 4a, as well as for other values of ms not shown here, that the flow breaks from the fully aerated jet (equation (4)) and asymptotically approaches the fully supported jet flow, πqb (5), as πe gets larger. For a particular geometry, we can approximate aerated jet flow with πqa = a1 + a2·πe and supported jet flow with πqb = b1 + b2·πe. If this is true, then as πe goes to infinity, πd → (a1-b1) + (a2-b2) ·πe. But this is not the same as (7). If we fit (7) to the data in Figure 4, πq will become negative as πe goes to infinity, an invalid, non-physical result. Either α changes with πe, or the proper equation for (7) is nonlinear.

Unfortunately, we have little choice with this data set. In Figure 4 there are 3 or 4 points out of 7 in the b = 0.2 m data that fall into the "partially supported jet" flow regime, but only 1 out of 6 for the b = 0.4 m data. This is typical. There are only 1, 2 or 3 points out of 6 for the b = 0.4 m data that fall into this restricted flow regime. That is not enough points to adequately define a nonlinear function when we have no sure knowledge of its form from other theory. We must use something as simple as (7) as a first approximation.

In hindsight, it may have been better to make the b = 0.2 m geometries the larger data set and measure b = 0.4 m to check scaling. Consider that in this experiment, the 0.2 m and 0.4 m breach models were run in the same flume, with a maximum depth of about 0.457 m (18 in) over the horizontal crest of the breach. At the most, the highest value of $\pi e$ for b = 0.4 m could be ½ that for b = 0.2 m for the same dimensionless geometry. For each breach width, the flow was set and the entrance head measured, and the range of flows was limited to the highest flow for the most restrictive breach. For b = 0.4 m, that limited the maximum depth for this geometry to about ½ that of the maximum depth for b = 0.2 m. So the maximum $\pi e$ for b = 0.4 m is about ¼ the maximum $\pi e$ for b = 0.2 m.

Froude scaling also dictates that the b = 0.2 m data set has larger relative scaled flows than b = 0.4 m data by a power of 5/2. This is also why the points for the b = 0.2 m data spread out over a much larger dynamic range than the b = 0.4 m data. Perhaps it would have been better to have performed this kind of dimensional analysis before the tests were too far along so that adjustments to the design could have been made.

Some of the longest strings of points in Figure 3 necessarily come from the data for b = 0.2 m, because of the scaling. Unfortunately, that data set is limited to only one value of mu. The

data set for b = 0.813m is even more restricted. So while it is tempting to use the data for b = 0.203m to fit (7), we will stick to the original experimental design, in which the data for b = 0.203m was meant only for checking scaling.

Scaling also poses another problem. There are only three values of $\pi h$, 0, 0.375 and 0.75, in the b = 0.406m data set. For the b = 0.203m data set, $\pi h$ = 0, 0.75 and 1.5. The same is true of $\pi u$. One can fit a curve to the range [0, 0.75], without any confidence that it will apply at 1.5. One cannot expect the b = 0.4 m data set, with such a small excursion into the partially-supported jet regime, to accurately estimate much larger scaled flows in the smaller b = 0.2 m data set.

Furthermore, it will become apparent that the data implies a lot of variation near $\pi h$ = 0, which cannot be resolved in any detail with the data that was taken. Three points is a very small set to use to define any function in terms of $\pi h$ or $\pi u$. This analysis must therefore be considered preliminary and subject to revision by future study.

There is also a slight difficulty in using (7) to estimate $\pi q$ when $\pi h$ = 0. The correction for $\pi u$ in $\pi qa$ (4) will still be calculated when $\pi h$ = 0, but it does not exist in (5). It is obvious that the correction must change with $\pi h$, but with so few points to resolve the matter, it is not clear how. This effect will remain unaccounted and ignored in this paper.

The analysis begins by fitting $\pi 0$ and $\alpha$ in (7) with simulated annealing to the measured ($\pi e$,$\pi q$) data points geometry by geometry. The objective function, fopt, in (8) is minimized. Like the dimensionless discharge coefficients, c0 and c1, in (3), $\pi o$ and $\alpha$ are assumed to be constant with $\pi e$. This is true often enough to produce reasonable fits.

$$fopt = \frac{1}{n}\sum_{i=1}^{n}\left|\frac{p\,\hat{q}_i - p\,q_i}{\sqrt{p\,\hat{q}_i \cdot p\,q_i}}\right| = \frac{1}{n}\sum_{i=1}^{n} rel_i \qquad (8)$$

The results are plotted and fitted against the π-variables, mu, ms, πu and πh, with a commercial 3-D curve fitting program to suggest parts of composite functions for the discharge coefficients, c0 and c1. Trial functions are then fitted to the b = 0.406m data set, and values of rel (8) are calculated for each (πe,πq) data point, along with the mean and standard deviation of rel.

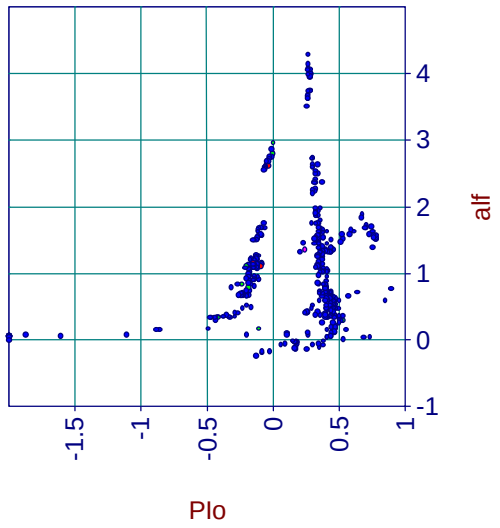


Figure 5: Plot of (πo, α) fitted to (7) for all data sets; $1.44(10^{-7}) \le rel \le 0.1147$, mean rel = 0.008342, standard deviation (std) rel = 0.013136

Figure 5 shows the first such plot using simulated annealing separately on all the geometries. The string of points for πo < 0 is associated mostly with πh = 0. The largest horizontal branch, at about 1 < α < 2, in the remaining string is from the b = 0.203m data set.

Figures 6a and b show πo and α fitted to the entire data set with some generic transition and peak functions, as a function of (mu, πh), the π-variables that have the strongest effects on these parameters. Notice the large amount of variation near πh = 0. Notice the data for b =

0.203m and πh = 1.5 sitting in a single spot to the left of the larger b = 0.406m data set. There is no data for mu ≠ 3 at πh = 1.5. That makes fitting any function of (mu, πh) in that region problematic.

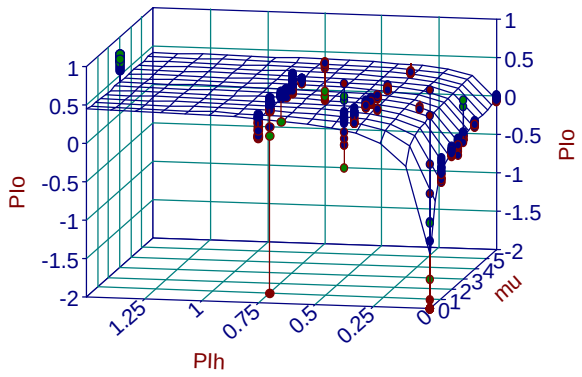


Figure 6a: πo(mu,πh) for individual fits to all geometries, fitted with 3-D transition function, $r^2$ = 0.71

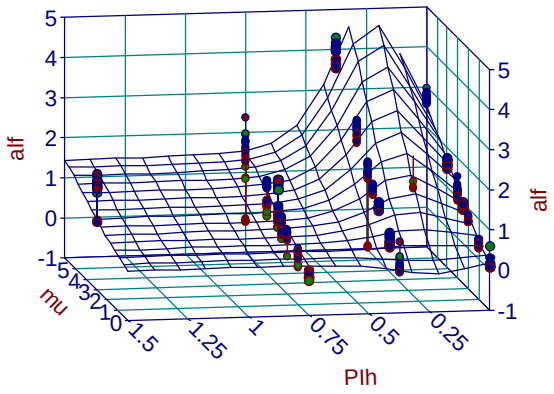


Figure 6b: α(mu,πh) for individual fits to all geometries, fitted with 3-D peak function, $r^2$ = 0.86

Notice also that there is a huge spread in πo at the point (mu, πh) = (0,0). This may be because the value of α varies about zero at this point. But why this should be the case here and not at πh = 0.375 and 0.75 is not well understood. Since this point is adequately addressed by equation (4), these data points are removed from the b = 0.406m data set in all further analysis.

Notice the large variation of α with πh over a wide range of mu. This is problematic for any assumption that α does not change with πe and that πq for πh ≠ 0 approaches πqb as πe goes to infinity. Consider that equation (7) also applies to πqb (9).

$$p_{qb} = \begin{cases} p_{qa} & ,p_e \le p_{ob} \\ p_{qa} - a_b(p_e - p_{ob}) & ,p_e > p_{ob} \end{cases} \qquad (9)$$

As πe goes to infinity and becomes much larger than either πo or πob, this implies that α must also approach αb for πq to approach πqb. This is obviously not the case implied by Figure 6b. One can force α to be invariant with πh and see how the results compare to cases where α is allowed to be a function of πh. But it is not clear how to use the available data to resolve this issue when it is so clearly limited in terms of both πe (typically 6 measurements) and πh (three settings).

It turns out that if α is held to be invariant in πh then the main effect of geometry upon it is a quadratic in mu (10). After some trial and error, one can find that most of the variation in πo in this case can be expressed by a simple rational function of mu and πh (11).

$$a = d6 + d7 \cdot mu + d8 \cdot mu^2 \tag{10}$$

$$p_o = \frac{d1 + d2 \cdot mu + d3 \cdot p_h}{1 + d4 \cdot mu + d5 \cdot p_h} \tag{11}$$

Using simulated annealing these equations were fitted simultaneously to (7) for all of the geometries and model data for which b = 0.406m and (mu, πh) ≠ (0,0). The objective function in equation (8) was minimized. This produced d1 = -0.53089, d2 = 0.0063986, d3 = 2.8973, d4 = 0.41199, d5 = 2.2271, d6 = 0.091873, d7 = 0.23883, d8 = 0.032078, with $0 \le rel \le 0.4059$, mean rel = 0.039667 and std rel = 0.04035. Figures 7a and 7b show the plots of (10) and (11).

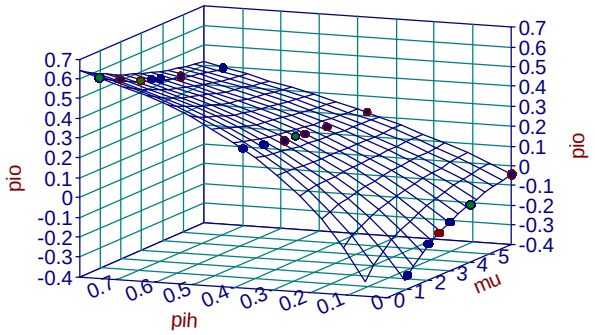


Figure 7a: πo versus (mu,πh) for equation (11), the simplest fit

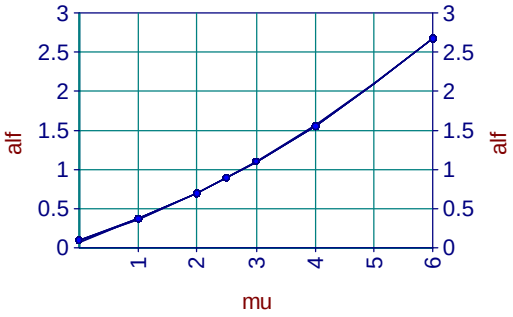


Figure 7b: α(mu) for equation (10), the simplest fit

Notice that when a general equation is fitted to all the relevant data, the mean and standard deviation of the relative absolute error is much greater than when the parameters α and πo are allowed to vary with each geometry (mean rel = 0.008342, standard deviation (std) rel = 0.013136). Figures 8a and 8b show the fits of πq-hat to πq and Q-hat to Q for this case. Notice that this approach overestimates the flow for the largest flows, where most of the points that deviate from aerated flow reside.

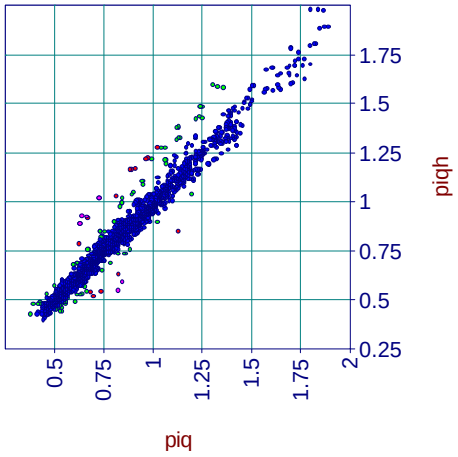


Figure 8a: πq-hat versus πq for equations (10) and (11), the simplest fit

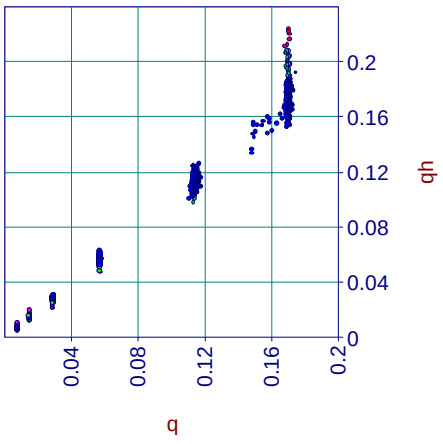


Figure 8b: Q-hat versus Q ($m^3/s$) for equations (10) and (11), the simplest fit

If α is allowed to vary with both mu and πh, then one eventually finds that the simplest set of equations is (11) and (12). This time simulated annealing produces a fit with d1 = -0.6011, d2 = 0.067015, d3 = 5.0276, d4 = 0.52844, d5 = 6.6795, d6 = 0.037756, d7 = 0.29284, d8 = 0.13106, d9 = -0.053821, d10 = -1.4806, d11 = 2.8593, with 0 ≤ rel ≤ 0.4286, mean rel = 0.036666 and std rel = 0.039307. Figures 9a and 9b show the plots of (11) and (12) with these parameters.

$$a = \frac{d6 + d7 \cdot mu + d8 \cdot p_h}{1 + d9 \cdot mu + d10 \cdot p_h + d11 \cdot p_h^2} \qquad (12)$$

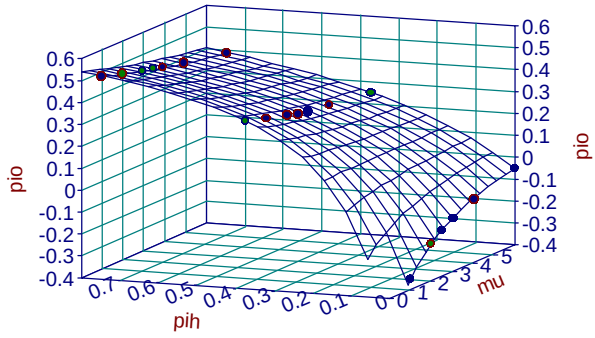


Figure 9a: πo versus (mu,πh) for equation (11)

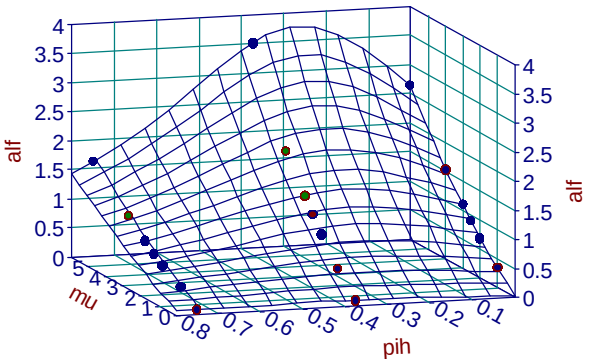


Figure 9b: α versus (mu,πh) for equation (12)

Figures 10a and 10b show the fits of πq-hat to πq and Q-hat to Q for this case. Notice that the outlier strings paralleling the main string of points in Fig. 8a have shrunk in 10a, and that the overestimation of flow in Fig. 10b for large flow is not so extreme.

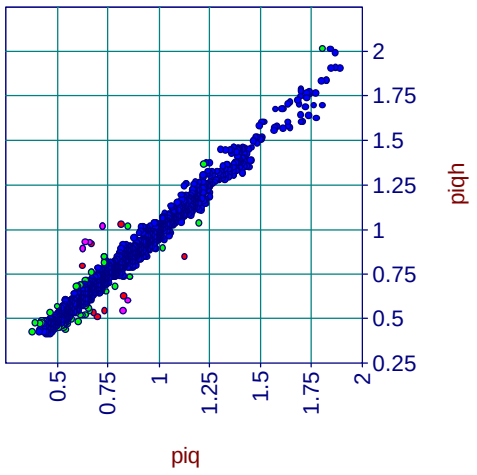


Figure 10a: πq-hat versus πq for equations (11) and (12)

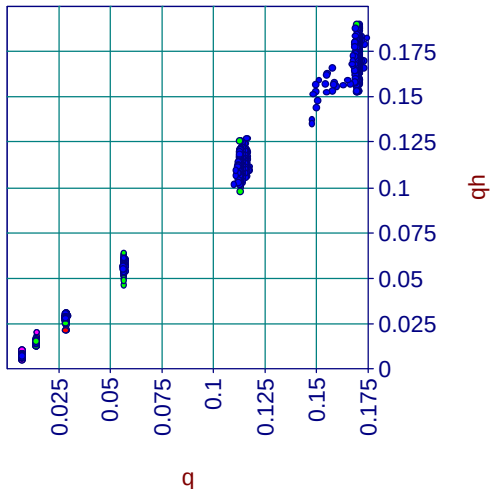


Figure 10b: Q-hat versus Q ($m^3/s$) for equations (11) and (12)

We can investigate any remaining variation in the fit by adding corrections to (11) and (12), as in (13), and using simulated annealing to fit the corrections, a1 and a2, to each geometry separately.

$$p_o = a1 + \frac{d1 + d2 \cdot mu + d3 \cdot p_h}{1 + d4 \cdot mu + d5 \cdot p_h}$$
$$a = a2 + \frac{d6 + d7 \cdot mu + d8 \cdot p_h}{1 + d9 \cdot mu + d10 \cdot p_h + d11 \cdot p_h^2} \qquad (13)$$

Without going through all the plots and details, suppose that we find that equations (14) and (15) seem likely to produce an improvement. Here we keep most of the fitted parameter values for (11) and (12), allowing variation in the parameters, d8 and d18, that produce the offsets from zero.

$$p_o = d1 \cdot mu + d2 \cdot mu^2 + d3 \cdot ms + d4 \cdot p_u + d5 \cdot p_h + d6 \cdot p_h^2 + d7 \cdot p_u \cdot p_h + \frac{d8 + 0.067015 \cdot mu + 5.0276 \cdot p_h}{1 + 0.52844 \cdot mu + 6.6795 \cdot p_h} \qquad (14)$$

$$a = d9 \cdot mu + d10 \cdot mu^2 + d11 \cdot mu \cdot ms + d12 \cdot ms + d13 \cdot ms^2 + d14 \cdot p_u + d15 \cdot mu \cdot p_h + d16 \cdot p_h + d17 \cdot p_h^2 + \frac{d18 + 0.29284 \cdot mu + 0.13106 \cdot p_h}{1 - 0.053821 \cdot mu - 1.4806 \cdot p_h + 2.8593 \cdot p_h^2} \quad (15)$$

Simulated annealing was used to fit (14) and (15) to the entire data set of b = 0.406m and (mu, πh) ≠ (0,0). This produced d1 = -0.021065, d2 = 0.031120, d3 = 0.0020986, d4 = -0.0069919, d5 = 0.074653, d6 = -0.030200, d7 = -0.010551, d8 = -0.48490, d9 = -0.017860, d10 = 0.0031367, d11 = 0.051211, d12 = -0.030200, d13 = 0.032915, d14 = 0.041426, d15 = -0.019616, d16 = 0.016088, d17 = -0.0012800, d18 = 0.046866, with with 0 ≤ rel ≤ 0.3796, mean rel = 0.033144 and std rel = 0.036863.

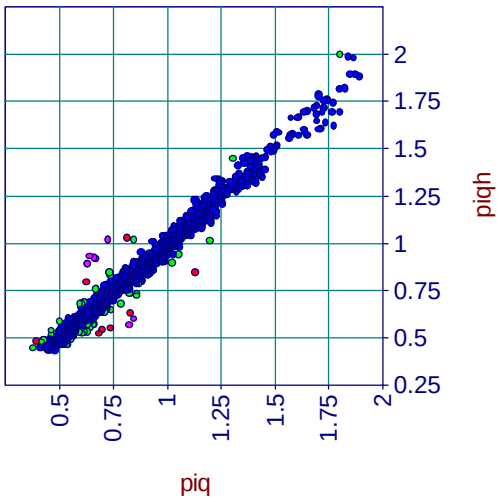


Figure 11a: πq-hat versus πq for equations (14) and (15)

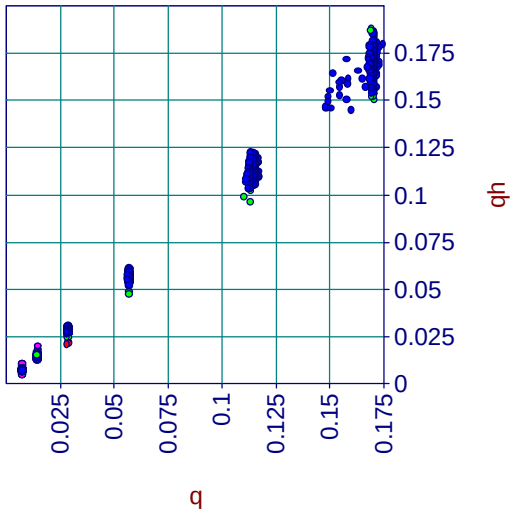


Figure 11b: Q-hat versus Q ($m^3/s$) for equations (14) and (15)

Figures 11a and 11b show the fits of πq-hat to πq and Q-hat to Q for this case. Although the reduction in the mean rel is statistically significant, with a z-score of 3.04, there is little visible improvement in the plots of estimated to measured flow.

## Results

For all of the Q(he) data measured in the physical model experiment, five different estimated flows, Q (m3/s), were calculated from (3): 1) Qa, from the aerated jet flow in (4), 2) Qb from the fully supported jet flow in (5), 3) Qc from the fit for partially-supported jets in (10) and (11) applied to (7), 4) Qd from the fits in (11) and (12), and 5) Qe from the fits in (14) and (15). For each measured and estimated flow pair, the absolute relative error (16) was also calculated.

$$rel_i = \left| \frac{\hat{Q}_i - Q_i}{\sqrt{\hat{Q}_i \cdot Q_i}} \right| \qquad (16)$$

Table 1 shows the statistics of rel (16) for b = 0.2, 0.4 and 0.8 m and πh = 0. The Q-column shows which equation applies. In the πe column, 1 designates results for which πe < πo and 2 results for which πe ≥ πo, where πo is calculated according to the fit of Qc, Qd or Qe. The remaining columns are the minimum, maximum, mean, standard deviation and number of rel in each row. Notice that according to (7), Qa is used when πe < πo.

Table 1: Absolute relative error statistics for πh = 0

b = 0.2 m

| Q | πe | min | max | mean | std | n |
|---|---|---|---|---|---|---|
| a | * | 0.0715 | 2.0470 | 0.9683 | 0.3835 | 120 |
| b | * | 0.0003 | 0.8140 | 0.0659 | 0.1157 | 120 |
| a | 1 | * | * | * | * | 0 |
| a | 1 | * | * | * | * | 0 |
| a | 1 | * | * | * | * | 0 |
| c | 2 | 0.0005 | 0.9979 | 0.1743 | 0.1538 | 120 |
| d | 2 | 0.0029 | 0.9805 | 0.1611 | 0.1482 | 120 |
| e | 2 | 0.0009 | 0.7242 | 0.1899 | 0.1225 | 120 |

b = 0.4 m

| Q | πe | min | max | mean | std | n |
|---|---|---|---|---|---|---|
| a | * | 0.0529 | 2.2490 | 0.6475 | 0.3794 | 763 |

| | | | | | | |
|---|---|---|---|---|---|---|
| b | * | 0.0000 | 0.4757 | 0.0294 | 0.0416 | 763 |
| a | 1 | * | * | * | * | 0 |
| a | 1 | * | * | * | * | 0 |
| a | 1 | 0.0877 | 1.9870 | 0.9100 | 0.3949 | 140 |
| c | 2 | 0.0006 | 1.1180 | 0.2043 | 0.2202 | 763 |
| d | 2 | 0.0003 | 1.0180 | 0.1888 | 0.1775 | 763 |
| e | 2 | 0.0004 | 2.1140 | 0.1995 | 0.2691 | 623 |

b = 0.8 m

| Q | πe | min | max | mean | std | n |
|---|---|---|---|---|---|---|
| a | * | 0.4365 | 0.8875 | 0.6075 | 0.1556 | 12 |
| b | * | 0.0065 | 0.1317 | 0.0360 | 0.0392 | 12 |
| a | 1 | * | * | * | * | 0 |
| a | 1 | * | * | * | * | 0 |
| a | 1 | * | * | * | * | 0 |
| c | 2 | 0.1396 | 0.2645 | 0.1939 | 0.0369 | 12 |
| d | 2 | 0.1258 | 0.2478 | 0.1781 | 0.0361 | 12 |
| e | 2 | 0.2608 | 0.4229 | 0.3250 | 0.0542 | 12 |

In each case in Table 1, the data is best fit by Qb. The fit of Qd is a distant second. There is an inconsistency between the use of $\pi e \geq \pi o$ here and $\pi e > \pi o$ in (7). But since it is rare, if ever, that $\pi e = \pi o$, this is a minor flaw.

Table 2 shows similar statistics for ph > 0 for the rest of the experimental data. Notice that the mean rel is less than 0.10 for all cases where $\pi e < \pi o$ and Qa applies. For b = 0.2 m, Qc fits best for $\pi e \geq \pi o$. For b = 0.4 and 0.8 m, Qd fits best for $\pi e \geq \pi o$. The results for b = 0.2 m and 0.8 m and $\pi e \geq \pi o$, intended to test scaling, are disappointing. In none of those cases is the mean rel below 0.10. In the case of b = 0.8 m, notice that there are many fewer measurements, a maximum of 12 compared to about 760, than for b = 0.4 m. The b = 0.4 and 0.8 m data can be directly compared for $\pi h = 0.375$ for Qc and Qd. The t-scores are 3.171 and 1.170, respectively, and the degrees of freedom are 3 and 1, respectively. If one chooses the 5% significance level, then there is not enough data to establish a statistically significant difference between the mean rel values in either case with the two-tailed t-test. This is not so

true of the b = 0.2 m data. The results are quite different from similar π-scales for b = 0.4 m data. Here we see the practical effect of the scaling considerations discussed about Figure 4.

Table 2: Absolute relative error statistics for πh > 0

b = 0.2 m, πh = 0.75

| Q | πe | min | max | mean | std | n |
|---|---|---|---|---|---|---|
| a | * | 0.0011 | 1.3450 | 0.3178 | 0.3682 | 122 |
| b | * | 0.1610 | 1.1150 | 0.5614 | 0.2072 | 122 |
| a | 1 | 0.0011 | 0.3965 | 0.0567 | 0.0851 | 54 |
| a | 1 | 0.0011 | 0.3965 | 0.0567 | 0.0851 | 54 |
| a | 1 | 0.0011 | 0.3965 | 0.0637 | 0.0750 | 72 |
| c | 2 | 0.0017 | 0.3771 | 0.1570 | 0.1064 | 68 |
| d | 2 | 0.0021 | 0.7520 | 0.2841 | 0.2096 | 68 |
| e | 2 | 0.1778 | 0.8840 | 0.4507 | 0.1765 | 50 |

b = 0.2 m, πh = 1.5

| Q | πe | min | max | mean | std | n |
|---|---|---|---|---|---|---|
| a | * | 0.0009 | 0.9903 | 0.1552 | 0.2384 | 123 |
| b | * | 0.0715 | 1.2260 | 0.6916 | 0.2263 | 123 |
| a | 1 | 0.0009 | 0.4572 | 0.0533 | 0.0837 | 76 |
| a | 1 | 0.0009 | 0.4572 | 0.0520 | 0.0858 | 72 |
| a | 1 | 0.0009 | 0.4572 | 0.0530 | 0.0776 | 90 |
| c | 2 | 0.0017 | 0.3105 | 0.1039 | 0.1148 | 47 |
| d | 2 | 0.0006 | 0.8662 | 0.2502 | 0.2717 | 51 |
| e | 2 | 0.1214 | 0.9138 | 0.3800 | 0.2664 | 33 |

b = 0.4 m, πh = 0.375

| Q | πe | min | max | mean | std | n |
|---|---|---|---|---|---|---|
| a | * | 0.0001 | 1.0630 | 0.1221 | 0.1777 | 762 |
| b | * | 0.0723 | 1.0660 | 0.4727 | 0.1915 | 762 |
| a | 1 | 0.0001 | 0.3794 | 0.0388 | 0.0468 | 299 |
| a | 1 | 0.0001 | 0.3794 | 0.0374 | 0.0468 | 388 |
| a | 1 | 0.0001 | 1.0630 | 0.0944 | 0.1721 | 583 |
| c | 2 | 0.0011 | 0.3034 | 0.0694 | 0.0608 | 463 |
| d | 2 | 0.0000 | 0.2470 | 0.0623 | 0.0565 | 374 |
| e | 2 | 0.0002 | 0.7172 | 0.1022 | 0.1268 | 179 |

b = 0.4 m, πh = 0.75

| Q | πe | min | max | mean | std | n |
|---|---|---|---|---|---|---|
| a | * | 0.0001 | 0.3550 | 0.0366 | 0.0369 | 756 |
| b | * | 0.0703 | 1.3880 | 0.5539 | 0.2552 | 756 |
| a | 1 | 0.0001 | 0.3550 | 0.0313 | 0.0365 | 555 |
| a | 1 | 0.0001 | 0.3550 | 0.0316 | 0.0366 | 552 |

| | | | | | | |
|---|---|---|---|---|---|---|
| a | 1 | 0.0001 | 0.3550 | 0.0344 | 0.0355 | 694 |
| c | 2 | 0.0000 | 0.1367 | 0.0448 | 0.0344 | 201 |
| d | 2 | 0.0003 | 0.1139 | 0.0289 | 0.0225 | 204 |
| e | 2 | 0.0008 | 0.1077 | 0.0434 | 0.0307 | 62 |

b = 0.8 m, πh = 0.1875

| Q | πe | min | max | mean | std | n |
|---|---|---|---|---|---|---|
| a | * | 0.0141 | 0.2428 | 0.0893 | 0.0844 | 12 |
| b | * | 0.1468 | 0.5727 | 0.4320 | 0.1287 | 12 |
| a | 1 | * | * | * | * | 0 |
| a | 1 | 0.0141 | 0.1741 | 0.0829 | 0.0711 | 4 |
| a | 1 | 0.0141 | 0.1741 | 0.0589 | 0.0504 | 10 |
| c | 2 | 0.0141 | 0.2937 | 0.1684 | 0.0973 | 12 |
| d | 2 | 0.0185 | 0.2429 | 0.1616 | 0.0846 | 8 |
| e | 2 | 0.1943 | 0.2009 | 0.1976 | 0.0047 | 2 |

b = 0.8 m, πh = 0.375

| Q | πe | min | max | mean | std | n |
|---|---|---|---|---|---|---|
| a | * | 0.0071 | 0.1707 | 0.0452 | 0.0474 | 12 |
| b | * | 0.1507 | 0.7305 | 0.4872 | 0.1808 | 12 |
| a | 1 | 0.0071 | 0.1707 | 0.0559 | 0.0556 | 8 |
| a | 1 | 0.0071 | 0.1707 | 0.0505 | 0.0505 | 10 |
| a | 1 | 0.0071 | 0.1707 | 0.0452 | 0.0474 | 12 |
| c | 2 | 0.0939 | 0.1949 | 0.1475 | 0.0490 | 4 |
| d | 2 | 0.1268 | 0.1389 | 0.1329 | 0.0085 | 2 |
| e | 2 | * | * | * | * | 0 |

**Conclusions**

Converting the weir equation to a linear dimensionless form, with $\pi q = Q/(g\ b^2\ he^3)^{1/2}$ and $\pi e = he/b$, clearly demonstrates where the $\pi q(\pi e)$ data deviates from that of flow through an aerated, freely-falling jet in a physical model of dam breach. The supposition that this occurs because of the rise of the reverse roller and the loss of aeration cannot be proved or disproved with this data set. Examination of the data taken for a breach width of b = 0.2 m tends to support the contention that as πe goes to infinity, the deviation from aerated jet flow causes the flow to approach that of fully-supported jet flow asymptotically, in a nonlinear fashion.

Unfortunately, the data set taken at a breach width of b = 0.4 m to calibrate theory and equations has a much smaller dynamic range compared to the much smaller data set at b = 0.2 m, taken to validate scaling. There are only 1, 2 or 3 data points for which the deviation is apparent in each breach geometry in the larger data set. This and the rudimentary nature of the theory limit the approximation of the deviation from aerated flow to a two-parameter linear equation, which in some cases will produce non-physical results in the limit of large $\pi e$.

Fitting this approximation also suggests that there is significant change in both deviation parameters, $\pi o$ and $\alpha$, as the dimensionless head cut height, $\pi h$, approaches zero. Unfortunately again, there is not enough data taken to clearly resolve the form of this change.

Nevertheless, simulated annealing is shown to be a powerful method of making these fits in the b = 0.4 m data set. When the fits are made separately to each geometry, assuming that the deviation parameters are constant with pe, the mean absolute relative error is 0.83% with a standard deviation of 1.3%. These fits show that the deviation parameters are high dependent on the upstream slope of the embankment, mu, and the height of the head cut, $\pi h$, beyond the horizontal crest of the breach notch in the upstream embankment. For reasons not clearly understood, the parameters are poorly defined for (mu, ph) = (0,0). These data points were removed for the fits to general equations.

With the anomalous data removed, fits of three general equations of increasing complexity and polynomial and rational polynomial form were made with simulated annealing. The mean absolute relative error for all the points, aerated and deviated, was minimized. The results were mean errors of 4.0, 3.7 and 3.3% for equations of increasing complexity. When only the points of deviation were considered the mean errors for the most effective general fitted

equations were 6.2% for b = 0.4 m and πh = 0.375 and 2.9% for b = 0.4 m and πh = 0.75. In all cases where the equation for aerated flow applied, the mean error was less than 10.0%.

Unfortunately, the fits to the data sets intended for validation, for b = 0.2 m and b = 0.8 m, were not so good. There were too few points in the 0.8 m data set to make any statistical conclusions at the 5% significance level. The results for the 0.2 m data set ranged from mean errors of 10.4% to 45.1% for the various equations applied to deviations, demonstrating a failure to predict. But these results were expected, because of the limited dynamic range of the calibration set and the use of a linear approximation to the deviation from aerated flow.

This suggests that the physical model experiment, or some reasonable computer simulation, needs to be redone, with an emphasis on resolving the form of the equation for the deviation from aerated flow. Future work also needs to clarify the dependence of the parameters of that equation on the head cut height, and to a lesser extent on the drop from the horizontal breach crest to the upstream reservoir floor. It hindsight, it may have been productive to have conducted this kind of analysis during the data taking, so that adjustments could have been made to the experimental design. It would have been better to have taken the calibration data set from b = 0.2 m models, or to have at least run the 0.4 m models brim full in every geometry.

## Acknowledgements

This is a complete reworking and extension of analysis done while the author was a postdoctoral associate at the USDA-ARS Hydraulic Engineering Research Unit in Stillwater, OK. The author did not take any of the physical measurements and appreciates the efforts of

Mr. Bob Sappington and Mr. Kevin Cook of the HERU in bringing him up to speed on the data. The author thanks the Agricultural Research Service for the opportunity to expand his horizons. 

## References

Baker, D.L. (2002). "Head-Discharge Equations to Fit a Set of Physical Models of Dam Breach". Submitted.

Fread, D.L. (1984). "A breach Erosion Model for Earthen Dams". Proceedings of Specialty Conference on Delineation of Landslides, Flash Flood, and Debris Flow Hazards in Utah. Utah State University, June 15, 30 pp.

Fread, D.L. (1991). "BREACH, An erosion model for earthen dam failures. (Revision 1, August 1991)" http://www.nws.noaa.gov/oh/hrl/rvrmech/documentation/breach.pdf

Goffe, W.L., G.D. Ferrier and J. Rogers (1994). "Global optimization of statistical functions with simulated annealing". Journal of Econometrics, 60(1/2):65-99.

Gupta, R.S. (1989) *Hydrology and Hydraulic Systems*. Waveland Press, Prospect Heights, IL.

John, J.A.E. and W.L. Haberman (1988). *Introduction to Fluid Mechanics*, Prentice Hall, Engelwood Cliffs, NJ.

Logan, J.D. (1987). *Applied Mathematics: A Contemporary Approach*. J. Wiley & Sons. New York.

Rand, W. (1955). "Flow geometry at straight drop spillways". Proc. Amer. Soc. of Civil Engineers, Vol. 8, No. 791.